Design, fabrication, and analysis of a 3DOF, 3cm flapping-wing MAV

R.J. Wood
School of Engineering & Applied Sciences
Harvard University
Cambridge, MA 02138
rjwood@eecs.harvard.edu

***Abstract*— Significant advances in meso-scale prototyping are enabling rigid, articulated, and actuated microrobotic structures. Here, an elegant manufacturing paradigm is employed for the creation of a biologically-inspired flapping-wing micro air vehicle with similar dimensions to Dipteran insects. A novel wing transmission system is presented which contains one actuated and two passive degrees of freedom. The design and fabrication are detailed and the performance of the resulting structure is elucidated highlighting two key metrics: the wing trajectory and the thrust generated.**

I. Introduction

The development of recent microfabrication technologies has enabled complex, robust, high performance articulated microstructures. This has fueled research into novel mechanisms on a 'meso'-scale; that is, mechanisms with feature sizes ranging from micron to centimeter. It is a natural progression to begin recreating some biological structures at-scale; something that has never before been possible. For example, researchers at U.C. Berkeley [1], [2] have made the initial attempts to create a two-winged robotic insect based upon a new manufacturing paradigm called Smart Composite Microstructures [3], [4]. Similarly, there have also been attempts to create a crawling robot the size of a cockroach using a similar approach [5].

This paper describes the design, fabrication, and analysis of a 3cm wingspan micro air vehicle (MAV) loosely based upon the morphology of insects of the order Diptera (more specifically, hoverflies of the family Syrphidae). Stated quite simply, the overall goal of this paper is to create a flapping-wing MAV that has a maximal lift-to-weight ratio. Little heed is given to issues such as controllability or sensing: this work is purely a stepping-stone on the path toward autonomous flying robotic insects.

II. Design

Dipteran insects drive their wing using indirect flight muscles attached to the exoskeleton dorsally and a deformable section of the exoskeleton call the scutum ventrally. Muscle activation works to depress the scutum while the pleural wing process is attached to the interface of the scutum and exoskeleton. This structure, shown in Fig. 1, is actuated by two sets of muscles: the dorsoventral and dorsolongitudinal muscles. The dorsoventral muscles act to depress the scutum and thus generate the 'up-stroke'. The dorsolongitudinal muscle acts to shorten the thorax and return the scutum to its relaxed state and thus generates the 'down-stroke' [6], [7].

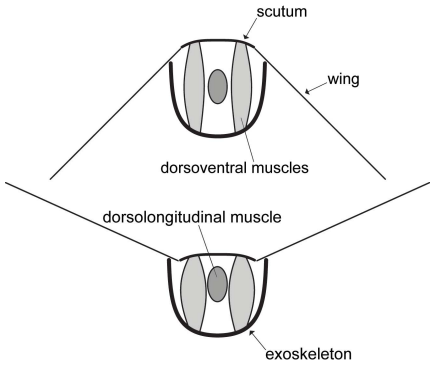

Fig. 1. Simplified diagram of Dipteran wing transmission (adapted from [8]).

Kinematically, the structure in Fig. 1 is essentially a four-bar with a prismatic joint at the input. What is presented here is nearly identical: linear actuator motion is coupled to the wing hinge via a simple transmission which acts to convert this motion to a large flapping rotation at the wing hinge. Thus all the actuator power is used to drive the wings through as large a wing stroke as possible. This is described in sec. II-A. Additionally, the wings are allowed to rotate along an axis parallel to the span-wise direction. This rotation is passive, but is key to generating lift and will be described in the sec. II-C. The design presented here diverges significantly from previous work at this scale (for example [9]) in the sense that there is only one actuated DOF in the entire system. There are similarities with work done by Goldfarb on MAVs with one or two actuated DOFs and tuned compliant DOFs (for example [10], [11]), however the mechanics presented here are one hundred times smaller.

A. Thorax kinematics

A transmission mechanism is used to transform small actuator motions to large angular wing displacements and to impedance-match the actuator to the load (work

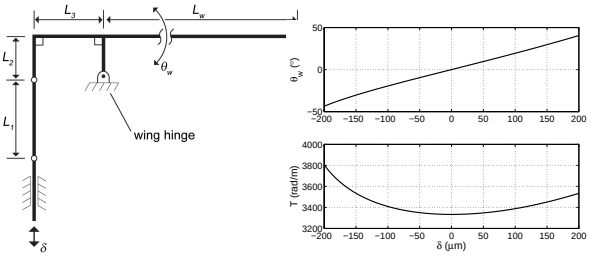

(a) (b)

Fig. 2. Kinematics of the transmission system (a) and analysis of system kinematics (b). Here, δ represents the actuator input and θ_w is the wing stroke angle.

done on the surrounding air). There are numerous reasons a large wing stroke is desired: for a given operating frequency a larger stroke amplitude will result in larger instantaneous wing velocities. Also, a larger stroke allows vortices to fully form and stabilize before the stroke reversal. At a 'macro' scale, this would be accomplished with a gear system. At the scale of an insect, it is not feasible to produce gears with the necessary efficiency, thus an alternative solution is presented here that is based on low-loss flexure joints. The basic mechanism is shown in Fig. 2(a) and the forward kinematics are defined by the following:

$$\theta_w = \cos^{-1}\left(\frac{\delta^2 - 2\delta L_1 + 2L_3^2}{2L_3\sqrt{(L_1-\delta)^2 + L_3^2}}\right) + \tan^{-1}\left(\frac{L_3}{L_1-\delta}\right) - \frac{\pi}{2} \quad (1)$$

While this expression is useful in calculating the full nonlinear dynamic model of the system, it is not terribly useful as a design tool. What would be ideal is to express the ratio of output angular displacement to the input linear displacement as a transmission ratio (analogous to a gear ratio). Although it is not possible to analytically solve equ. (1) for this ratio, it can be seen that when δ and θ_w are small we can make the following approximation:

$$T \equiv \frac{\theta_w}{\delta} \approx \frac{1}{L_3} \quad (2)$$

We refer to T as the transmission ratio. This is solved for numerically (shown in Fig. 2(b)) and is approximated for use as a design tool using equ. (2). For example, if we desire the largest possible wing motion for a given actuator motion, T should be as large as possible, or equivalently L_3 should be as small as possible. Given the constraints of the current construction method, links less than 250μm in length are not feasible and this is used as the lower limit. Thus for $L_3 = 300\mu$m (see Fig. 4), $T \approx 3300\text{rad}\cdot\text{m}^{-1}$ resulting in a wing deflection of $\pm 60^\circ$ for an actuator input of $\pm 300\mu$m.

The value of L_1 is chosen by observation of equ. (1). Intuitively, as $L_1 \to 0$ the four-bar becomes a three-bar and the transmission is singular. As $L_1 \to \infty$ equ. (1) becomes:

$$\lim_{L_1 \to \infty} \theta_w = \sin^{-1}\delta \quad (3)$$

This implies that as L_1 grows large, $T \to 1$. To ensure a compact structure, L_1 is chosen to be 500μm.

The last parameter of significance in Fig. 2(a) is the length L_2. For compactness, L_2 should be as small as possible. However it cannot be zero since proper joint alignment at the 'rest-state' is crucial to the dynamics of articulated flexure-based structures [12].

It should be noted that the motion of the distal end of the bending cantilever actuator is not actually linear. Instead, the motion forms an arc and this motion needs to be converted into the linear motion δ at the input to the transmission system. This is a trivial component that is solved with a 2-link slider-crank mechanism similar to that discussed in [3].

B. Dynamics

The dynamics of the wing and transmission system are crucial for the overall performance of the system. For efficiency, the actuator, transmission, and wings form a resonant structure such that the motion of the wing is amplified when driven at resonance (in the case that the system is under-damped). Wing rotation will be discussed below, however it is noted here that the wing flapping is driven at resonance and the passive rotation occurs quasi-statically. Since the work done on the air is approximately proportional to the wing velocity squared, along with maximizing the stroke angle it is desirable to maximize the resonant frequency. To model the resonant frequency, an energy method is used that takes into account the potential and kinetic energy of the system. First, to derive the potential energy, it is noted that there are *n*+1 elastic energy storage mechanisms in this structure: the actuator and the *n* joints of the transmission. The model for the actuator (discussed below) gives the stiffness in the actuator reference frame. Each of the joint deflections are determined in their own coordinate frame and thus there is no need to transform the motion of each joint onto some inertial reference frame. Since each joint's motion is fully defined by the forward kinematics, we can simply sum the potential energies of each joint:

$$U_{tot} = U_a + \sum_{i=1}^{n} U_i \quad (4)$$

where U_a is the potential energy elastically stored in the actuator due to a forced deflection and U_i are the flexure

potential energies. These terms are given as follows:

$$\begin{aligned} U_i &= \tfrac{1}{2} k_i \gamma_i^2 \\ U_a &= \tfrac{1}{2} k_a \delta^2 \end{aligned} \tag{5}$$

The k_i terms are the actuator rotational stiffnesses ($= EI/l_i$), k_a is the actuator stiffness, γ_i are the joint deflections, and δ is the actuator motion. Finally, the potential energy can be used to estimate an equivalent stiffness, k_{eq}, by taking partial derivatives as was detailed in [4]. The kinetic energy of the system is overwhelmingly dominated by the wing inertia [13]. This greatly simplifies the calculation of the total system kinetic energy by allowing the user to ignore the contributions of the individual links. Instead, the kinetic energy is simply:

$$K_{tot} = K_w + K_{\text{air}} = \frac{1}{2} \left(J_{yy} + J_{\text{air}} \right) \dot{\theta_w}^2 \tag{6}$$

where K_w is the kinetic energy of the wing and K_{air} is the kinetic energy due to the added mass of the trapped air (virtual mass). While it is feasible to calculate the inertia of the wing directly, due to potentially complex shapes it is much more convenient to use a mechanical modeling tool (e.g. SolidWorks, see Fig.3(a)) to give a numerical estimate. The added mass effect is estimated using the following:

$$dm = \frac{\pi \rho}{4} c\left(x\right)^2 dx \tag{7}$$

where x is the span-wise direction, $c\left(x\right)$ is the chord at x, and ρ is the density of air [8]. Integrating this will give the virtual mass added to the wing, however, we are more interested in the inertia of the wing for a rotation about the wing hinge. Thus equ. (7) can be modified as follows:

$$J_{\text{air}} = \iiint_V r^2 dm = \frac{\pi \rho}{4} \int_0^l c\left(x\right)^2 x^2 dx \tag{8}$$

Using the model airfoil shown in Fig. 3(a) we can directly estimate the resonant frequency as $\omega_n = \sqrt{k_{eq} / \left(J_{yy} + J_{\text{air}} \right)}$ (the inertias are defined by the coordinate system in Fig. 3(a)). It should be noted that this resonant frequency is for the linearized system. To account for nonlinear system dynamics, a similar approach could use the potential and kinetic energies and internal (loss) and external (load) dissipations in an Euler-Lagrange formulation.

C. Airfoil and wing hinge

It is beyond the scope of this paper to introduce either analytical or numerical modeling for a given airfoil. Instead, the design of the planform shape of the airfoil simply mimics Dipteran insects. The remaining parameters of the wing design have the following goals:

TABLE I

GEOMETRIC AND INERTIAL PARAMETERS OF THE WING.

mass (mg)	mass[1] (mg)	len. (mm)	chord[2] (mm)
0.50	0.20	16	3.13
area[2] (mm^2)	J_{yy}[3] (mg·mm^2)	J_{xx}[3] (mg·mm^2)	J_{air}[1] (mg·mm^2)
50	24.20	0.95	5.23

[1] virtual
[2] average chord
[3] mass moment of inertia

reduce the flapping inertia as much as possible, tune the rotational inertia, and maintain wing rigidity.

The second and third degrees of freedom in the system are the respective rotations of each wing. The wing pronation and supination (collectively the wing rotation since the stroke is assumed to be symmetrical for hovering flight), are passive in this design. During the translational phase of the wing stroke, aerodynamic loading applies a torque on the wing that tends to decrease the angle of attack ϕ. In this design, a flexure allows passive rotation along an axis parallel to the span-wise direction. To ensure that this rotation does not exceed an optimal angle, joint stops are incorporated as part of the flexure. This is shown in Fig. 3(b). The

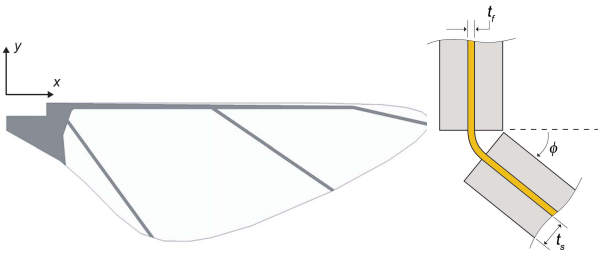

(a) (b)

Fig. 3. Drawing of the airfoil vein and membrane structure (a) and diagram of the wing rotation and joint-stop mechanism (b).

geometry of the flexure defines the limits of the flexure joint motion (and the maximum angle of attack):

$$\phi_{max} = \frac{\pi}{2} - \frac{L_f}{t_s} \tag{9}$$

where ϕ is the geometric angle of attack. Since wing rotation bends the flexure, potential energy is stored during the stroke and is released at the end of stroke to further accelerate rotation in the opposite direction. This potential energy is converted into a kinetic energy at the transition between each half stroke, and we can equate these two energies to give the rotational velocity (purely due to releasing this strain energy):

$$\dot{\phi} = \omega_r \phi_{max} \tag{10}$$

where $\omega_r = \sqrt{k_r/J_{xx}}$. It should be noted that this is only the velocity due to the stored strain energy in the rotational flexure. There is also aerodynamic loading and wing inertia that will force the wing to rotate at the start of each half-stroke. It should also be noted that quasi-static passive wing rotation will only occur with a wing drive frequency significantly below ω_r.

D. Actuation

The flight muscle is a bimorph piezoelectric bending cantilever optimized for high energy density [14], [15]. These actuators have been successfully integrated into other microrobotic devices such as in [5], [3], [16]. The actuator is based upon a laminate plate theory model of a layered structure in which some of the laminae are electroactive. Thus an internal stress develops upon the application of an electric field generating a bending moment. See [14] for details on the modeling and design of such actuators. These systems have numerous benefits over other morphologies: high bandwidth, simple geometry and actuation, low loss, and simple fabrication. However, there are drawbacks as well including low fracture toughness and high magnitude electric field.

III. Fabrication

Because of the size constraints on the constituent components, traditional manufacturing paradigms are inappropriate for the construction of the articulated structures that will make up the transmission. Wood et al described a solution to creating rigid, articulated, and actuated microstructures with micron-scale features called Smart Composite Microstructures (SCM) [4]. This process involves laminated laser-micromachined materials arranged in arbitrary 2D patterns. An individual lamina can be virtually any material with a range of properties chosen to give a desired compliance profile.

A. Transmission

Construction of the transmission is an exceedingly crucial step. As was shown in the above analysis, the kinematics and dynamics of the transmission depend strongly upon the concise geometry of each link and flexure. Additionally, the assumption that we can use a pseudo-rigid-body technique assumes that all joints are properly aligned.

To put this in perspective, the smallest link in the transmission system is 300μm in length and the flexure lengths are 80μm. Alignment is controlled by the precision stages of the laser-micromachining system. Fig. 4 shows the resulting transmission system which converts a small linear motion to large angular wing strokes.

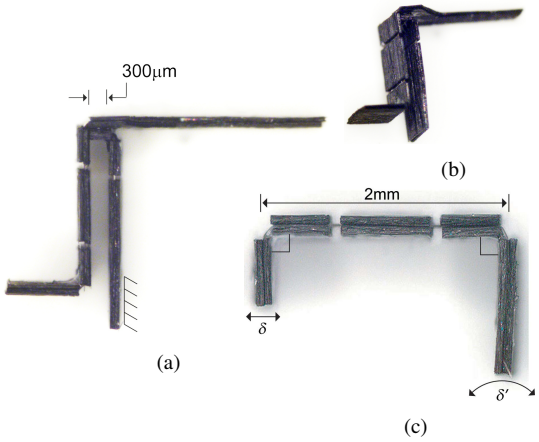

Fig. 4. MAV transmission system, top view (a) and isometric view (b). The slider-crank for coupling actuator motion to the prismatic input of the transmission is shown in (c). Here δ' is the actuator motion and δ is the resulting linear input.

B. Actuation

The actuators are also constructed using the SCM process. In this case, some of the laminae are piezoelectric, thus resulting in bending moments upon the application of an electric field. Tab. II gives relevant properties and Fig. 5 shows a completed microactuator.

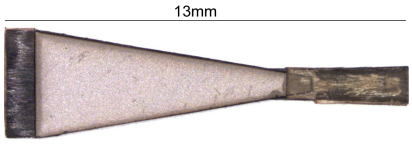

Fig. 5. High energy density piezoelectric bending cantilever.

TABLE II
MEASURED AND ESTIMATED ACTUATOR PARAMETERS.

mass (mg)	deflection[1] (μm)	stiffness[2] (Nm^{-1})
40	438	467

force[1,2] (mN)	energy dens.[2] (Jkg^{-1})	ω_n[2] (kHz)
135	1.5	2.56

[1]peak
[2]estimated

C. Airfoil

The airfoils are constructed using the SCM process to cut the reinforcing 'veins' and the membrane. To maintain wing rigidity, the fiber orientation of the veins is a key concern. To address this, the veins are individually cut and aligned to a predetermined pattern. This is then cured to the membrane between teflon sheets and released giving the structure shown in Fig. 6.

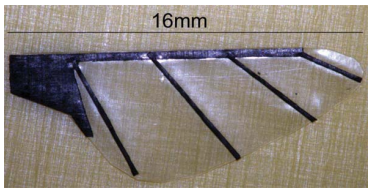

Fig. 6. Completed airfoil highlighting vein structure.

The membrane is 1.5μm thick polyester and the veins are cut from a 70μm thick ultra-high modulus carbon fiber/epoxy composite sheet.

IV. Analysis

While the obvious figure of merit for the complete structure is the lift that is produced, an intermediate metric is the trajectory that the wings achieve. Both will be quantified here, and neither are particularly simple to discern.

A. Integration

The actuator, wings, and transmission are assembled together onto an acrylic fixture that is created with a three dimensional printer. Care is given to the strength of the mounts so that a solid mechanical ground is established. Detail of the completed structure is shown in Fig. 7. This mount is used in place of an airframe that will be developed for future versions.

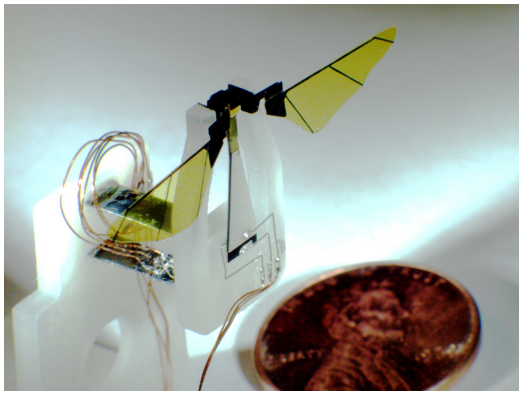

Fig. 7. Completed MAV test fixture mounted to a high sensitivity force transducer.

B. Wing trajectory

Development of the wing trajectory is conceptually simple. The actuated DOF is driven through as large a motion as possible. This is done open-loop with a sinusoidal drive at the resonant frequency. The measured resonant frequency is 110Hz, resulting in an actuator power density of approximately 165Wkg^{-1} (comparable to good macro-scale DC motors). This is lower than the predicted resonant frequency of 170Hz, most likely due to unmodeled offsets in how the wing is mounted to the transmission. Fig. 8 details the wing motion that this structure can achieve. Note that this motion is qualitatively identical to hovering Dipteran insects.

C. Wing force

Because of the small force magnitude and high operating frequency, measuring the thrust produced by the wings in real time (with sub-period temporal resolution) is not trivial. A custom sensor was created specifically to measure this force. The design attempts to reconcile two opposing traits: high bandwidth and high sensitivity. To quantify this, the bandwidth of the sensor is desired to be at least 5$\times$ the wing drive frequency with a resolution of less than 1% of the weight of the structure. For the details of the design, the reader is directed to [17]. The sensor itself is a parallel cantilever constructed from spring steel with semiconductor strain gages. The completed sensor has a resonant frequency of 400Hz (with the structure attached; slightly lower than desired), and a resolution of approximately 10μN.

The structure is fitted to the distal end of the sensor and the device is actuated, starting from rest. The average lift is measured by averaging 50 wing beats after 50 wing beats are elapsed to allow stable periodic vortex formation. The average lift was collected from 10 trials giving an average of 1.14$\pm$0.23mN. This would be sufficient to lift a fly weighing over 100mg. A typical time trace of the lift is shown in Fig. 9 for a drive magnitude of 100V peak.

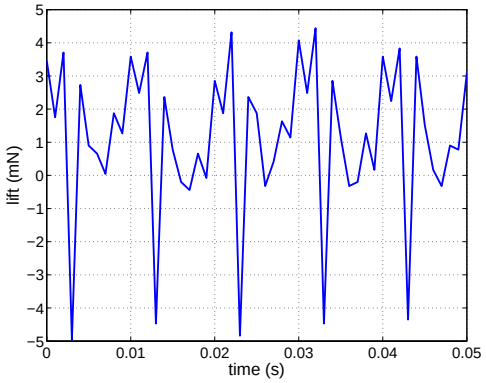

Fig. 9. A typical lift trace.

V. Discussion

The transmission morphology presented here has shown merit in the generation of lift force for a flapping wing MAV. Other than the relative simplicity of having one actuated DOF, the use of a central power actuator is a scalable architecture that will be expanded upon in future revisions.

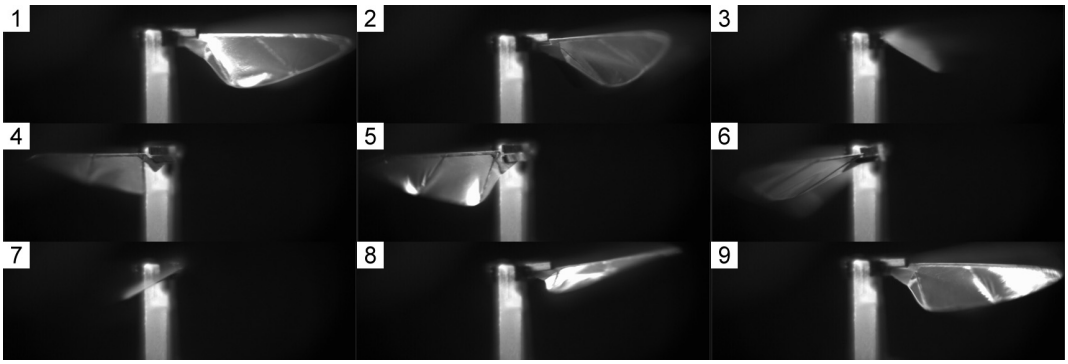

Fig. 8. Example wing motion with passive rotation.

There is a trade-off between limited control of wing motion and the size and complexity of the actuation and transmission: concisely controlling the wing stroke may result in greater propulsive efficiency, but will likely result in a more massive system. Clearly, this MAV design is under-actuated and cannot produce arbitrary body torques. As a solution, smaller actuators will be added to the structure to actively tune the dynamics by dissipating or injecting energy into the wing stroke on a sub-period basis with bilateral asymmetry. Again, this is directly analogous to how actual insects efficiently modulate body moments.

Stability and control are critical issues to address for future autonomous insect-sized MAVs. There is a dichotomy between stability and maneuverability that is manifest in the agility of insect flight. Creating a structure that is passively stable will impede the maneuverability of a MAV, but will alleviate some of the complexity inherent in the controller topology. Alternatively, an insect-like MAV will be extremely unstable such that the smallest stroke asymmetry will cause huge angular accelerations due to minuscule body inertias [18]. This establishes a monumental control challenge (when considering electrical and processing power limitations), but could also be exploited to create a remarkably agile flyer.

ACKNOWLEDGEMENTS

Thanks to the Dickinson lab at Caltech, and the Fearing lab at U.C. Berkeley for helpful discussions.

REFERENCES

[1] R. Fearing, K. Chang, M. Dickinson, D. Pick, M. Sitti, and J. Yan, "Wing transmission for a micromechanical flying insect," in *IEEE Int. Conf. on Robotics and Automation*, Apr. 2000.

[2] J. Yan, R. Wood, S. Avadhanula, and M. S. amd R.S. Fearing, "Towards flapping wing control for a micromechanical flying insect," in *IEEE Int. Conf. on Robotics and Automation*, Seoul, Korea, May 2001.

[3] R. Wood, S. Avadhanula, M. Menon, and R. Fearing, "Microrobotics using composite materials: The micromechanical flying insect thorax," in *IEEE Int. Conf. on Robotics and Automation*, Taipei, Taiwan, Sept. 2003.

[4] R. Wood, S. Avadhanula, R. Sahai, E. Steltz, and R. Fearing, "Microrobot design using fiber reinforced composites," *to appear: J. of Mechanical Design*, 2007.

[5] R. Sahai, S. Avadhanula, R. Groff, E. Steltz, R. Wood, and R. Fearing, "Towards a 3g crawling robot through the integration of microrobot technologies," in *IEEE Int. Conf. on Robotics and Automation*, Orlando, FL, May 2006.

[6] W. Gronenberg, "Fast actions in small animals: springs and click mechanisms," *J. Comp. Physiology A*, vol. 178, pp. 727–734, 1996.

[7] J. Miyan and A. Ewing, "Is the 'Click' Mechanism of Dipteran flight an artefact of CCl_4 anaesthesia?" *J. of Experimental Biology*, vol. 116, pp. 313–322, 1985.

[8] R. Dudley, *The Biomechanics of Insect Flight: Form, Function and Evolution*. Princeton University Press, 1999.

[9] S. Avadhanula, R. Wood, D. Campolo, and R. Fearing, "Dynamically tuned design of the MFI thorax," in *IEEE Int. Conf. on Robotics and Automation*, Washington, DC, May 2002.

[10] A. Cox, D. Monopoli, D. Cveticanin, M. Goldfarb, and E. Garcia, "The development of elastodynamic components for piezoelectrically actuated flapping micro-air vehicles," in *J. of Intelligent Material Systems and Structures*, vol. 13, Sept. 2002, pp. 611–615.

[11] A. Cox, D. Monopoli, M. Goldfarb, and E. Garcia, "The development of piezoelectrically actuated micro-air vehicles," in *SPIE Conf. on Microrobotics and Microassembly*, vol. 3834, Boston, Massachusetts, Sept. 1999, pp. 101–108.

[12] S. Avadhanula and R. Fearing, "Flexure design rules for carbon fiber microrobotic mechanisms," in *IEEE Int. Conf. on Robotics and Automation*, Barcelona, Spain, Apr. 2005.

[13] S. Avadhanula, R. Wood, E. Steltz, J. Yan, and R. Fearing, "Lift force improvements for the micromechanical flying insect," in *IEEE/RSJ Int. Conf. on Intelligent Robots and Systems*, Las Vegas, Nevada, Oct. 2003.

[14] R. Wood, E. Steltz, and R. Fearing, "Optimal energy density piezoelectric bending actuators," *J. of Sensors and Actuators A: Physical*, vol. 119, no. 2, pp. 476–488, 2005.

[15] ——, "Nonlinear performance limits for high energy density piezoelectric bending actuators," in *IEEE Int. Conf. on Robotics and Automation*, Barcelona, Spain, Apr. 2005.

[16] D. Campolo, R. Sahai, and R. Fearing, "Development of piezoelectric bending actuators with embedded piezoelectric sensors for micromechanical flapping mechanisms," in *IEEE Int. Conf. on Robotics and Automation*, Taipei, Taiwan, Sept. 2003.

[17] R. Wood and R. Fearing, "Flight force measurements for a micromechanical flying insect," in *IEEE/RSJ Int. Conf. on Intelligent Robots and Systems*, Maui, HI, Oct. 2001.

[18] S. Fry, R. Sayaman, and M. Dickinson, "The aerodynamics of free-flight maneuvers in *Drosophila*," *Science*, vol. 300, pp. 495–498, Apr. 2003.